Impact of Atomic Oxygen on the Structure of Graphene Formed on Ir(111) and Pt(111)

ARTICLE *in* THE JOURNAL OF PHYSICAL CHEMISTRY C · APRIL 2011

Impact Factor: 4.77 · DOI: 10.1021/jp111962k

7 AUTHORS, INCLUDING:

Nikolay A Vinogradov
MAX IV Laboratory
32 PUBLICATIONS **382** CITATIONS
SEE PROFILE

Anders Mikkelsen
Lund University
156 PUBLICATIONS **2,794** CITATIONS
SEE PROFILE

Edvin Lundgren
Lund University
231 PUBLICATIONS **5,795** CITATIONS
SEE PROFILE

Alexei Preobrajenski
Lund University
89 PUBLICATIONS **1,680** CITATIONS
SEE PROFILE

THE JOURNAL OF PHYSICAL CHEMISTRY C

ARTICLE

pubs.acs.org/JPCC

Impact of Atomic Oxygen on the Structure of Graphene Formed on Ir(111) and Pt(111)

N. A. Vinogradov,[†,‡] K. Schulte,[*,‡] M. L. Ng,[†,‡] A. Mikkelsen,[§] E. Lundgren,[§] N. Mårtensson,[†,‡] and A. B. Preobrajenski[*,‡]

[†]Department of Physics, Uppsala University, Box 530, 75121 Uppsala, Sweden

[‡]MAX-lab, Lund University, Box 118, 22100 Lund, Sweden

[§]Division of Synchrotron Radiation, Department of Physics, Lund University, Box 118, 22100 Lund, Sweden

ABSTRACT: The effect of atomic oxygen adsorption on the structure and electronic properties of monolayer graphite (MG or graphene) grown on Pt(111) and Ir(111) has been studied using X-ray photoelectron spectroscopy, near-edge X-ray absorption fine structure spectroscopy, and scanning tunneling microscopy. For comparison, the adsorption of atomic oxygen on highly oriented pyrolytic graphite has been studied under the same conditions. Graphene oxidation predominantly occurs through the formation of epoxy groups and causes atomic-scale buckling of the graphene lattice, as evidenced by an sp^2-to-sp^3 bonding transformation. The different parts of the graphene/metal moiré superstructure show different oxidation dynamics, with the initial formation of epoxy groups in the more bonding "pores". Upon O adsorption, the nearest C neighbors of epoxy groups get engaged in a stronger bonding with the substrate. As a result, the pores of the graphene mesh become attracted and effectively pinned to the substrate by the O atoms. A limited intercalation of oxygen under graphene is also probable. Annealing of the samples after oxygen exposure only partially recovers the original graphene structure and results in the formation of a dense pattern of quasi-periodic, nanometer-sized holes. Both the selective oxidization and the hole formation can be exploited for selective functionalization or tuning of the electronic properties.

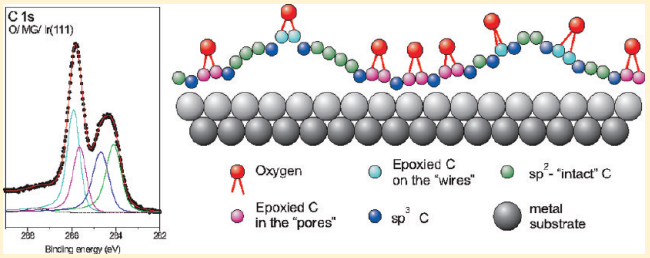

INTRODUCTION

The awarding of the 2010 Nobel prize in physics for the discovery of two-dimensional graphene emphasizes the rapid growth and enormous importance of this new area of research, launched only shortly before in 2004.[1] The reason for graphene's popularity is clear: its remarkable physical and chemical properties make it attractive not only for fundamental physics research but also for fabricating novel electronic devices (sensors, transistors[2,3]), hydrogen storage and hydrogen-based energetics,[4,5] and for material science and catalysis.[6−11] Ironically, to make graphene capable of replacing silicon—the current staple of microelectronics—efforts are needed toward controllably disturbing the perfect conduction properties of graphene and introducing a (tunable) band gap to achieve semiconducting behavior. A number of approaches have so far been pursued; for example, the gap can be induced and controlled by an external electrical field in bilayer graphene[12] or can be created by quantum confinement in graphene nanoribbons.[13−16] Alternatively, band-gap opening can be achieved by a direct contact of graphene with other materials, including (i) weakly adsorbing (physisorbed) particles that can introduce a modest, reversible perturbation,[17,18] (ii) modification of the interaction between certain substrates and graphene through intercalation of molecular species or atoms that preferentially interact with the substrate,[19,20] and even (iii) through using more covalently bonding (chemisorbed) species, such as H, OH, or F. The latter approach can considerably influence and even disrupt (at high coverage) the π band of graphene, as a result of eliminating the double-bond contribution to the C−C bonds and the sp^2-to-sp^3 transformation.[21] It can, however, offer a robust and controllable way of modifying graphene's electronic structure, provided the mechanism behind the bonding process is elucidated.

Freestanding graphene is often corrugated and wrinkled in unpredictable ways, which can greatly affect its ability to form covalent bonds with adsorbates, which, in turn, will affect ultimate uptake values. Therefore, in order to better control the chemical modification, this degree of freedom can be constrained by using graphene with well-defined nonequivalent adsorption sites, such as graphene films grown on suitable lattice-mismatched substrates.[22−24] The periodically corrugated graphene monolayers can be formed by catalytic decomposition of hydrocarbons on the close-packed metal surfaces, such as Ru(0001),[25,26] Rh(111),[22,27] Ir(111),[28−30] and Pt(111).[31] As the strength of chemical interaction with graphene is growing in the series Pt−Ir−Rh−Ru,[22] graphene is locked in registry with the substrate on Ru(0001) and Rh(111) but can form a variety of coexisting

Received: December 16, 2010
Revised: March 12, 2011
Published: April 22, 2011

rotational domains and different moiré structures on Pt(111).[31] On Ir(111), graphene grows mainly with one domain orientation and with a remarkable long-scale perfection,[29,30] although admixtures of other orientations were also observed.[32] The periodic nanometer-scale corrugation of a graphene layer on lattice-mismatched substrates can be used for a controllable growth and ordering of metal clusters with a very narrow size distribution.[27,28,33]

For electronic applications, it is important that a significant band-gap opening can be achieved by chemical functionalization, as was exemplified by hydrogenation of graphene on Ir(111), which is largely reversible through annealing.[21] In this context, atomic oxygen is perhaps an even more promising agent for purposeful chemical functionalization of graphene, as it is capable of forming stable bonds, but unfortunately can occur in more than one type of bonding (e.g., ether, epoxide, ketone). This is also known from graphene oxide (GO), which is an insulator accommodating several oxygen species (C═O, C−O−C, COOH, OH) on both the basal planes and the edges of flakes.[34−37] It is mainly prepared ex situ in strong oxidizing solutions, making a clear determination of precise processes and contributions of the different oxygen-containing species difficult. In contrast, when the graphene oxidation process is studied on a metal substrate under ultra-high-vacuum conditions, the hydroxyl and carboxyl species can be readily ruled out due to the lack of hydrogen, and edge effects are strongly reduced, especially for graphene grown on iridium, which allows for a nearly perfect monolayer coverage.

Using atomic oxygen is crucial for chemical functionalization of graphene, because molecular oxygen is too inert to interact with graphitic surfaces at room temperature. Instead, elevated temperatures or pre-etching is needed to encourage interaction.[38,39] Indirect use of molecular oxygen can, however, be made by letting it decompose on the underlying substrate first, as in the MG/Ru(0001) system,[19,40−42] or by using ozone.[43] Surprisingly, there is a lack of experimental studies on the direct interaction of graphene with atomic oxygen, although oxidation of HOPG has been studied recently.[44] A number of theoretical studies on the oxygen−graphene interaction are also available, although they focus on the use of O_2 molecules[45] or free-standing graphene as a sample.[37,46−50] Individual O atoms are generally believed to adsorb on free-standing graphene in the form of epoxy (1,2-ether, not 1,3-ether) groups, while preferential arrangement of epoxy groups in lines was predicted and associated with unzipping effects.[46,51] In contrast, no sequential alignment of epoxies was observed in the recent transmission electron microscopy study of GO and reduced GO.[52]

Here, we report on the interaction of atomic oxygen with graphene grown on Pt(111) and Ir(111), studied by means of high-resolution X-ray core-level spectroscopies (HR CLS) and scanning tunneling microscopy (STM). On both surfaces, graphene is adsorbed rather weakly, yet somewhat stronger on Ir(111), resulting in a more pronounced periodic corrugation on the latter substrate.[22] The adsorption of atomic oxygen on graphene supported by the 5d transition metals (Pt, Ir) at room temperature is shown to result in drastic changes in the electronic and geometric structure of the graphene film. The adsorption process is described in terms of formation of the epoxy groups and a local rippling of the graphene film. A considerable influence of the Pt and Ir substrates on the oxidation process is observed as compared to adsorption of the same amount of oxygen on HOPG. Furthermore, the thermal stability of the oxidized samples is investigated and discussed.

EXPERIMENTAL DETAILS

All the spectroscopic measurements were carried out in situ at beamline D1011, MAX-Lab, Lund University, with the exception of the spectra reported in Figure 8, which were measured at beamline I311, MAX-lab, using similar sample preparation conditions. The surfaces of Pt and Ir single crystals were cleaned by several cycles of Ar^+ sputtering (ion energy = 1 kV, ion current = 2−5 μA), annealing at 900 °C, and oxygen treatment (whenever necessary) at a partial pressure of oxygen of 5×10^{-8} mbar and subsequent flashing for around 30 s at 1150 °C. The cleanliness of the substrate was verified spectroscopically by CLS as well as by means of LEED, showing no additional spots except those from the substrate. Graphene was grown by thermal cracking of propylene (C_3H_6) in contact with the hot metal surface at the temperature of around 1000 °C in the hydrocarbon partial pressure of 1×10^{-7} mbar. Prior to the heating, the surfaces were exposed to 60 L of propylene at room temperature (RT) to achieve the best graphene film quality and big sizes of grains. Cleaning of the highly oriented pyrolytic graphite (HOPG) sample was performed by cleaving it in situ and annealing to 600 °C. The samples were treated at RT by atomic oxygen produced in a commercial oxygen cracker (from MBE-Komponenten GmbH). The source was operated at T = 1650 °C, ensuring an efficient cracking of oxygen molecules without production of high-energy ions or material deposition from the filament or capillary onto the sample surface. The source was operated at an oxygen partial pressure of 1×10^{-7} mbar. All samples were characterized by photoelectron spectroscopy (PES), NEXAFS, and low-energy electron diffraction (LEED). However, the LEED patterns are not discussed in the present paper because neither additional spots nor a change of symmetry were ever detected, and only a gradual blurring of the patterns was observed with increasing O coverage, implying that the oxygen adsorption occurs randomly. The C K-edge NEXAFS spectra were measured in the partial electron yield mode (retarding potential U = −100 V) in order to increase the signal-to-background ratio. The photon energy resolution of the C 1s NEXAFS spectra was set to 75 meV, and the resolution of the C 1s PE spectra was 125 meV, at $h\nu$ = 350 eV. Both NEXAFS and PE spectra were accumulated at an angle of 50° between the light polarization vector and the surface normal, implying normal emission geometry. All NEXAFS spectra were normalized to the intensity of the incident radiation, and the photoelectron spectra were measured relative to the Fermi level of the corresponding substrate. The FitXPS software was used for the peak fit analysis of the PE spectra. The STM measurements were performed at RT on the samples prepared in a separate chamber equipped with a commercial UHV STM (STM1 from Omicron GmbH). Base pressure in the STM preparation chamber was better than 5×10^{-10} mbar and in the analytical chamber about 1×10^{-10} mbar. The WSxM software[53] was used for the STM image processing.

RESULTS AND DISCUSSION

Before discussing the spectra and phenomena related to the oxidation of graphene on transition metals (TMs), it is very instructive to consider first a more simple case: the oxidation of graphite. The C 1s PE spectrum of HOPG recorded with $h\nu$ = 350 eV before and after the oxidation is shown in Figure 1. The spectrum from pristine HOPG can be fitted with just one peak (C1) at the binding energy (BE) of 284.42 eV, while at low and intermediate O coverage, an additional peak (C2) develops at the

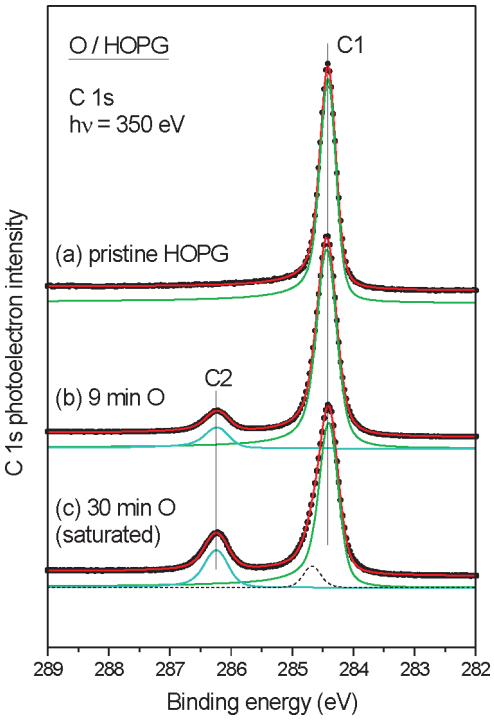

Figure 1. Evolution of the C 1s PE spectrum from HOPG upon adsorption of atomic oxygen. The spectra are recorded with $h\nu$ = 350 eV for high surface sensitivity.

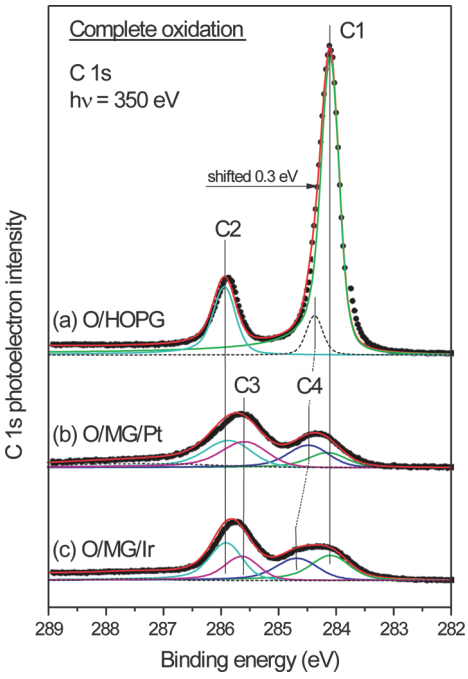

Figure 2. Impact of atomic oxygen on C 1s PE spectra from graphite (a) and graphene on Pt(111) (b) and Ir(111) (c). All spectra correspond to saturated oxidation. The spectrum from HOPG is shifted by 0.3 eV to lower BE to facilitate the comparison.

BE of 286.22 eV (relative shift = +1.8 eV). This is accompanied by an overall broadening of peak C1. These findings are in good agreement with the results of the recent study of oxidation of pristine and defective graphite by Barinov et al.[44] In this work, the authors assigned peak C2 to the formation of epoxy groups on the basal plane of graphite, while the broadening of peak C1 (which was handled by an additional component at lower BEs) was associated with the slight change of the chemical surrounding for the neighbors of those C atoms, which are directly involved in epoxy groups. We fully agree with this assignment, as the formation of other functional groups is less probable. Indeed, the C−OH hydroxyl groups (which are typical constituents of GO) are excluded in our experiments, and the C 1s PE signature of the −C═O carbonyl groups has an essentially different BE (287.8 eV).[54] Furthermore, C−O−C ether groups (with no bond between C atoms) can also be excluded on the basis of the O 1s PE spectrum (see Figure 7, part a), which shows only one component at 531.1 eV, with ether-related components expected at higher binding energies around 533.7 eV.[54] Thus, component C2 in Figure 1 can be confidently assigned to C−O−C epoxy groups (1,2-ether with a single bond between C atoms).

With increasing oxygen exposure, a new component gradually develops in the C 1s PE spectrum of O/HOPG at 284.65 eV and becomes pronounced close to the saturation limit (Figure 1, part c). It can hardly be associated with O-induced defects, as no new signatures of ketonic or ether groups appear in the C 1s or in the O 1s spectra. Therefore, we associate it with a slight buckling of those graphite atoms in the uppermost layer, which are not directly bound to oxygen.

In going from oxidized HOPG to oxidized graphene on 5d metal surfaces, Pt(111) and Ir(111), the impact on the C 1s PE spectrum is much more dramatic, as shown in Figure 2, parts b and c, for saturated oxidation. The peak assigned earlier to epoxy groups on O/HOPG (C2) is considerably broadened and can be described in terms of two contributions: one, analogous to oxidized graphite, at 285.9 eV (labeled C2) and a new peak at 285.6 eV (labeled C3). Peak C4 is also found on the metal substrates but is progressively shifted away from C1 toward higher BEs (+0.26 eV for O/HOPG, +0.37 eV for O/MG/Pt, and +0.59 eV for O/MG/Ir). On both Pt and Ir, the graphene is not matched to the substrate lattices, resulting in a weak periodic corrugation, which is more pronounced on Ir due to the stronger interaction between graphene and metal. The adsorption of O atoms on the bonding (closer to the metal surface, also called "pores") and less bonding (further from the metal surface, also called "wires") sites can slightly differ. Therefore, it is plausible to assign components C2 and C3 to the epoxy groups formed in these higher and lower sites, respectively. This assignment is based on the observation that C2 is separated from the original C1 component by 1.8 eV, just like in the case of epoxy groups on HOPG. Thus, it can be associated with the epoxy groups adsorbed on elevated, more free-standing, wires, while C3 is due to the same groups formed in the more interacting pores of corrugated graphene. Evidently, the separation of the PES signal from epoxy groups into contributions C2 and C3 is not strict and rather formal, as these peaks are not well-defined and can be treated also as either one broad signal or a collection of many peaks with small shifts. We also observed that the fitting of the C2−C3 separation at different oxygen exposures is more stable for O/MG/Ir than for O/MG/Pt. This is in agreement with the fact that graphene corrugation is more pronounced on Ir, whereas on Pt, different rotational domains and weaker corrugation hamper a strict separation of adsorption sites into two groups. Nevertheless, dividing the signal from epoxy groups into two major contributions is justified from a comparison with the

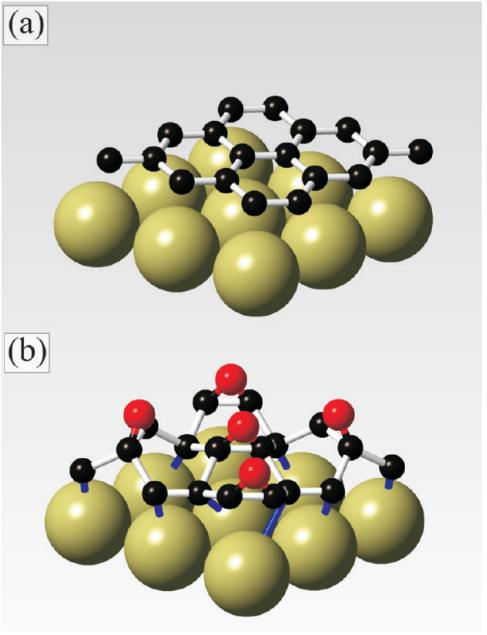

Figure 3. Schematic representation of graphene on a 5d TM surface in the so-called pore of the MG/TM moiré superstructure before (a) and after (b) adsorption of atomic oxygen. Black and red balls represent C and O atoms, respectively. Blue sticks visualize an increased bonding between the substrate and those C atoms that are not bonded to O.

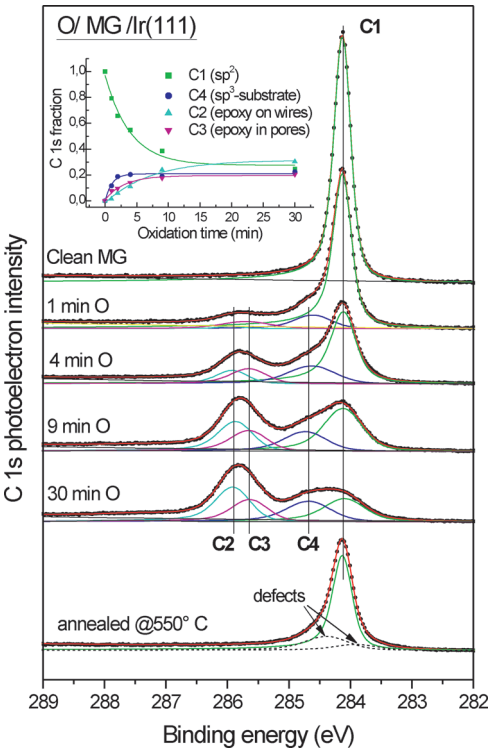

Figure 4. Evolution of the C 1s PE spectrum of graphene on Ir(111) as a function of increasing oxidation time up to the saturation level, and further annealing at 550 °C. Inset: intensity variation of individual components in the peak fit as a function of oxidation time. Solid curves in the inset are exponential fits to the experimental data represented by scattered symbols.

corresponding signal from O/HOPG (Figure 2) and fits well into the discussion of adsorption dynamics (see below).

Analogous to the case of O/HOPG, component C4 can be associated with the C atoms neighboring the epoxy groups, although influenced by the substrate. A similar spectral feature was also observed upon hydrogenating graphene on TMs, which is known to result in lifting the partial double-bond nature of the C−C bond and a local disturbance of the electron π system.[55] As this takes place, one of the two liberated electrons participates in the C−H bond, while the other one can contribute to increased bonding between neighboring C atoms and the substrate, leading to a strong buckling of the graphene film. The latter C atoms (involved in the C−TM bonding) are responsible for the C 1s component shifted by +0.5 eV from the original sp^2-related peak.[55] We believe that, in the case of oxygen adsorption, component C4 has the same nature, and the mechanism of graphene buckling on the atomic scale is similar, although formation of epoxy groups does not lead to the concentration of excessive electron density in the vicinity of the adsorption site in the form of an unpaired electron. Nevertheless, bonding of an O atom to two adjacent C atoms locally destroys conjugation of the π electron system of the graphene ring, leading to formation of localized π orbitals on the nearest C neighbors. It is plausible to assume that these localized orbitals readily mix with the TM 5d states, leading to increased C−TM bonding and attraction of these C atoms to the metal surface. As a result, the C atoms in epoxy groups become pushed upward while their neighbors are pulled downward, thus making graphene buckled. This is schematically illustrated in Figure 3, which show random adsorption of O atoms on the more bonding site of the graphene/TM interface (e.g., in the pore of the MG/Ir(111) superstructure). Blue sticks visualize a formation of the stronger C−TM bonds upon O adsorption. When O adsorption on MG/Ir and MG/Pt is compared, this effect is expected to be more pronounced for the stronger interacting MG/Ir system, which is indeed reflected in the growing separation of C4 from C1 in the series O/HOPG−O/MG/Pt−O/MG/Ir (Figure 2).

The transformation of the C 1s photoelectron spectrum in MG/Ir(111) upon successive oxidation steps is presented in Figure 4 alongside a spectrum obtained after annealing a fully oxygenated sample. Already, the first step of oxidation (1 min or 6 L (Langmuir)) results in clear changes in the C 1s spectrum shape, and all components observed at saturated oxygenation are present from the beginning. Upon further oxygen adsorption, features C2, C3, and C4 become more pronounced, at the expense of the signal from the pristine sp^2-bonded graphene (C1), indicating an increase in the number of carbon atoms involved into the oxidation process. Interestingly, the rate of growth/decline of these peaks is not the same for all four peaks. The inset in Figure 4 shows how the relative peak area of individual components contributing to the total C 1s intensity varies as a function of oxygen exposure. The intensity of peak C1 (referred to as "sp^2") exponentially decreases and reaches saturation at exposures around 100 L (approximately 17 min at the pressure used). In contrast, C4 (C atoms neighboring the epoxy groups, labeled "sp^3") reaches saturation very quickly, leveling out already around 18 L (3 min), indicating that the local buckling associated with oxidation in the pores occurs already at low oxygen coverage. Component C3 (epoxy C atoms in the graphene pores) reaches saturation at about 60 L (10 min), while C2 (epoxy C atoms on the wires) only just levels off at 100 L.

dx.doi.org/10.1021/jp111962k |J. Phys. Chem. C 2011, 115, 9568–9577

These oxidation dynamics support our assignment of the individual components. Indeed, somewhat shorter distances between graphene and metal atoms inside the pores make adsorption in the pores more favorable than on the wires, because localized π orbitals on the nearest C neighbors of the epoxy group can be easier engaged in the bonding with TMs, thus reducing the total energy. As a result, graphene in the pores is more likely to form a buckled conformation. This is the reason why C3 grows faster than C2 in the initial stage of oxidation. In contrast, wires are more similar to freestanding graphene with only one side exposed to particles and the other side relatively passive, making them less prone to the formation of epoxy groups than pores. However, at saturation, C2 dominates over C3, in agreement with the dominating presence of the nonbonding areas in MG/Ir.[22] In general, it can be suggested that oxidation starts from the pores and "nails" them to the substrate. This behavior resembles the adsorption dynamics of atomic hydrogen on graphene/TM interfaces[21,55] and possibly represents a universal course of behavior for any chemical functionalization of these systems. Lastly, it is plausible that C4 grows faster than C3 in the beginning, because one O atom adsorbed in a pore creates two C atoms in the epoxy group (C3) and four affected neighbor C atoms with increased interaction with the metal substrate (C4). As adsorption proceeds, the intensity ratio of C3/C4 is expected to evolve from 1:2 to the theoretical limit of 1:1 for the completely oxidized graphene pores, provided the nearest C neighbors of one epoxy group are buckled downward and cannot participate in another epoxy group. Indeed, the intensities of C3 and C4 are nearly equal at saturation (Figure 4, inset), thus confirming our assignment of their nature.

The spectrum from the oxygen-saturated MG/Ir sample annealed at 550 °C for 10 min is shown at the bottom of Figure 4. Upon annealing, peaks C2 and C3 start to decrease in height from about 150 °C and vanish completely around 350 °C, accompanied by a decline in feature C4. The return toward the original C 1s spectral shape, the recovery of the moiré pattern in LEED (not shown), and the absence of an O 1s signal after annealing all point to desorption of oxygen and a recovery of the graphene layer. The resultant peak, however, is significantly broadened and reduced in area to 50−60% compared to the C 1s obtained on pristine graphene on Ir(111). This means that part of the graphene layer has been etched away upon heating, most likely desorbing in the form of CO and/or CO_2,[56] and the remaining layer, therefore, contains defects that contribute to a spread in binding energies of the C 1s line. In Figure 4 (bottom), the spectral broadening is accounted for by two extra peaks at 284.37 eV (+0.23 eV off from the main peak) and 283.86 eV (−0.28 eV off from the main peak) associated with defects. This is very similar to the case of bulk graphite, where a variety of defect types can be responsible for the broadening of the C 1s PE signal.[44]

Figure 5 shows an evolution of the C 1s absorption spectrum in graphene from MG/Ir(111) (a) to slightly oxidized (b), moderately oxidized (c), and the oxygen-saturated sample (d), as well as the result of annealing of the latter sample to 550 °C (e). Already at the first step of oxidation, the NEXAFS spectrum is smeared out in the region of both the π^* and the σ^* states. This indicates changes in the atomic and electronic structure of graphene due to accommodation of the oxygen atoms and formation of the C−O−C bonds. The region of the π^* states shows considerable broadening, which can be associated with an increased C−Ir interaction as a result of the O-induced buckling of graphene in

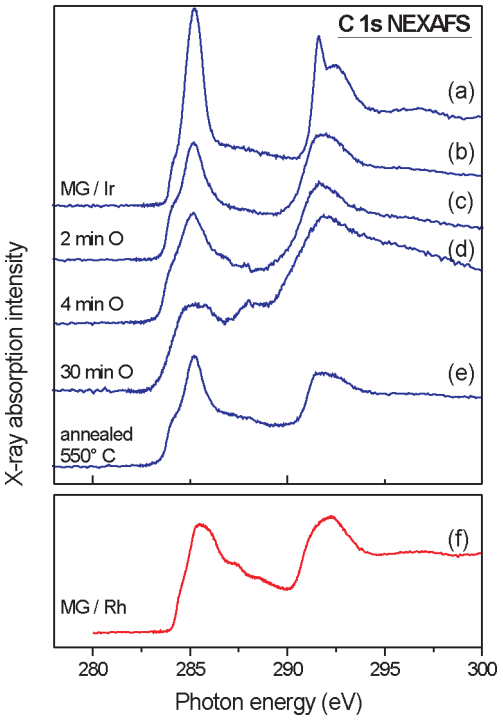

Figure 5. Evolution of the C 1s NEXAFS spectra from MG on Ir(111) as a function of atomic oxygen treatment and further annealing (a−e). C 1s NEXAFS of pristine graphene on Rh(111) (from ref 22) is shown in (f) for comparison.

the pores. Spectrum (c) in Figure 5 roughly corresponds to the situation when the pores are filled with epoxy groups and have become pinned to the metal substrate. The periodicity of the moiré structure observed in LEED was, however, not affected significantly. The resulting structure becomes strongly corrugated, resembling the nanomesh formed by pristine graphene on Rh(111) or Ru(0001).[22,23] This fact can be confirmed by the direct comparison with the C 1s NEXAFS spectrum from MG/Rh(111) shown in Figure 5f. This spectrum is a signature of strongly corrugated graphene on strongly interacting substrates, as it contains features corresponding to both bonding and nonbonding graphene sites.[22] An obvious similarity between the C 1s NEXAFS spectra (c) and (f) is an indication that the MG/Ir system becomes strongly pinned in the pores (i.e., corrugated) by the adsorption of atomic O. On the way to saturated oxidation, a new feature develops at 288 eV (Figure 5, spectrum d), which can be attributed to a small number of other species, possibly ether groups, because a pronounced feature at this energy was observed in the C 1s NEXAFS spectrum of dimethyl ether (CH_3-O-CH_3).[57] Removing oxygen by annealing to 550 °C (Figure 5, spectrum e) results in a partial recovery of the original spectral shape (a), but not completely, indicating a defective structure of the graphene adlayer, in agreement with the C 1s PE data above.

The emerging picture of graphene modification by atomic oxygen can be supported and further developed by STM. Figure 6a shows a characteristic image from a pristine MG/Ir sample, where individual graphene rings and a moiré structure resulting from the well-studied graphene corrugation[33] are visible. Exposing this surface to atomic oxygen leads to apparent changes in the surface structure. In Figure 6, images b−d correspond approximately to the oxygen dose of 4, 9, and 30 min used in the spectroscopic experiments, respectively (see Figure 4). An apparent

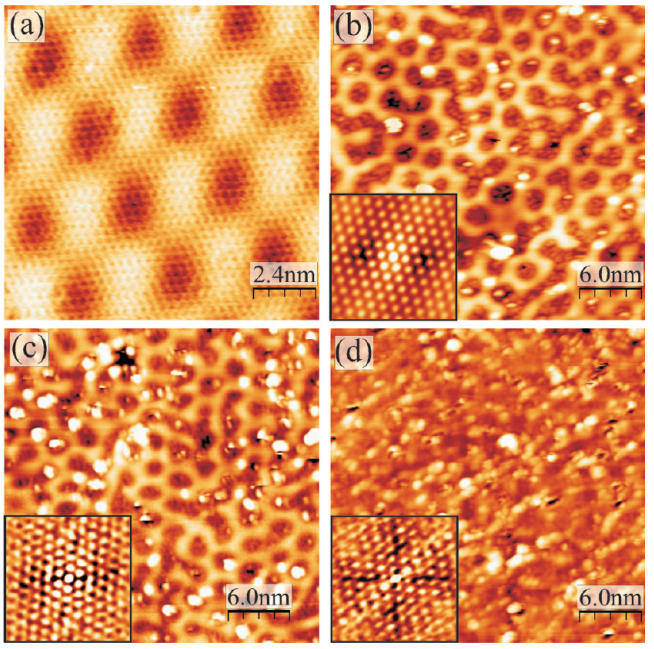

Figure 6. STM images of (a) atomically resolved pristine graphene showing the moiré structure and MG/Ir(111) samples upon low (b), moderate (c), and high (d) exposure to atomic O at RT. The insets in (b)−(d) show the autocorrelation pattern of these STM images. The tunneling parameters and sizes are V_{bias} = 1.2 V, I_t = 1 nA, 15 × 15 nm for (a), V_{bias} = 1.6 V, I_t = 150 pA, 30 × 30 nm for (b, c), and V_{bias} = 1.8 mV, I_t = 30 pA, 30 × 30 nm for (d).

degradation of the moiré periodicity is visible already in Figure 6b, with a number of pores connected to each other in an irregular manner. However, the overall periodicity is preserved, as can be seen from the autocorrelation pattern (inset) showing bright spots ordered in a 6-fold symmetry of the moiré pattern with the distances between the spots (≈2.7 nm) characteristic for the MG/Ir(111) superstructure.

Inside each pore, several bright protrusions can be seen (Figure 6a). The number of the bright spots increases with increasing oxygen dosage (Figure 6c). From the STM images alone, it is difficult to associate the bright spots with any oxygen-induced adsorbate or structure, without theoretical support. However, given that the HR CLS measurements presented above directly indicated the formation of epoxy groups on the surface under the same conditions, we attribute the bright spots to epoxy groups. This is in agreement with the atomically resolved STM studies of exfoliated graphene oxide by Pandey et al., where bright protrusions were also observed and associated with O atoms in the bridge positions.[58] The epoxy groups pin the graphene to the substrate, as described above. In contrast, no or very few epoxy groups could be identified in our STM images on the elevated parts of the moiré pattern, although a small number of very bright spots randomly scattered on the wires may represent such groups (Figure 6b,c). It was also not possible to directly detect O atoms on the reference HOPG surface oxidized in the same way. The reason may be a combination of low adsorption energy and unstable tunneling conditions. The difficulty in directly imaging epoxy groups on graphite was mentioned previously in the STM study of HOPG treated by oxygen plasma.[59] In the pores of the graphene, the epoxy groups appear to be more stable, as they can be easily visualized even at RT.

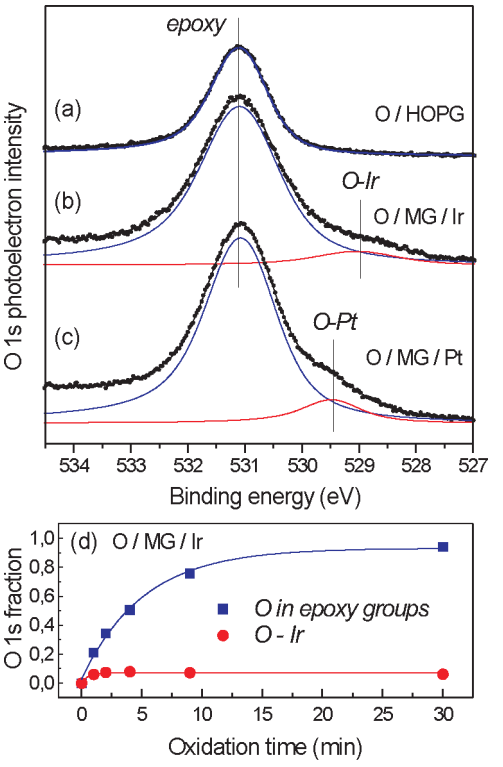

Figure 7. O 1s PE spectra of oxygen-saturated HOPG (a) and graphene on Ir(111) (b) and Pt(111) (c). Intensity variation of individual components in the O 1s PE spectrum of O/MG/Ir is shown in (d) as a function of oxidation time. Solid curves in (d) are exponential fits to the experimental data represented by scattered symbols.

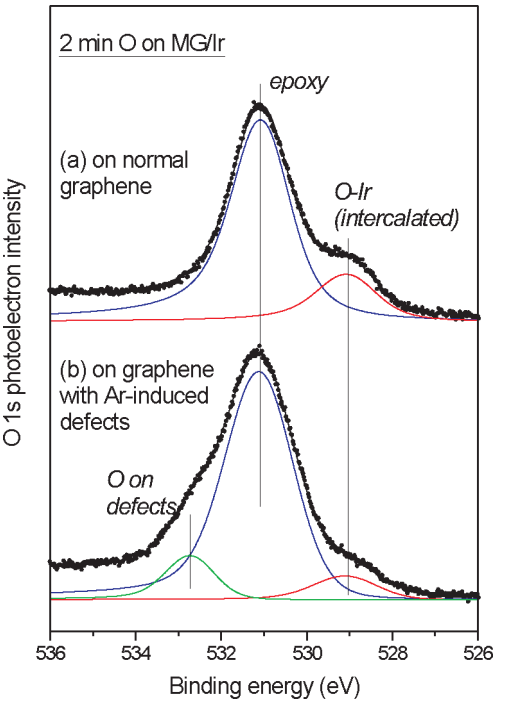

Figure 8. O 1s PE spectra from atomic oxygen adsorbed on (a) intact and (b) defective graphene on Ir(111). Point defects on graphene are introduced by mild and short sputtering with Ar^+ ions.

dx.doi.org/10.1021/jp111962k |J. Phys. Chem. C 2011, 115, 9568–9577

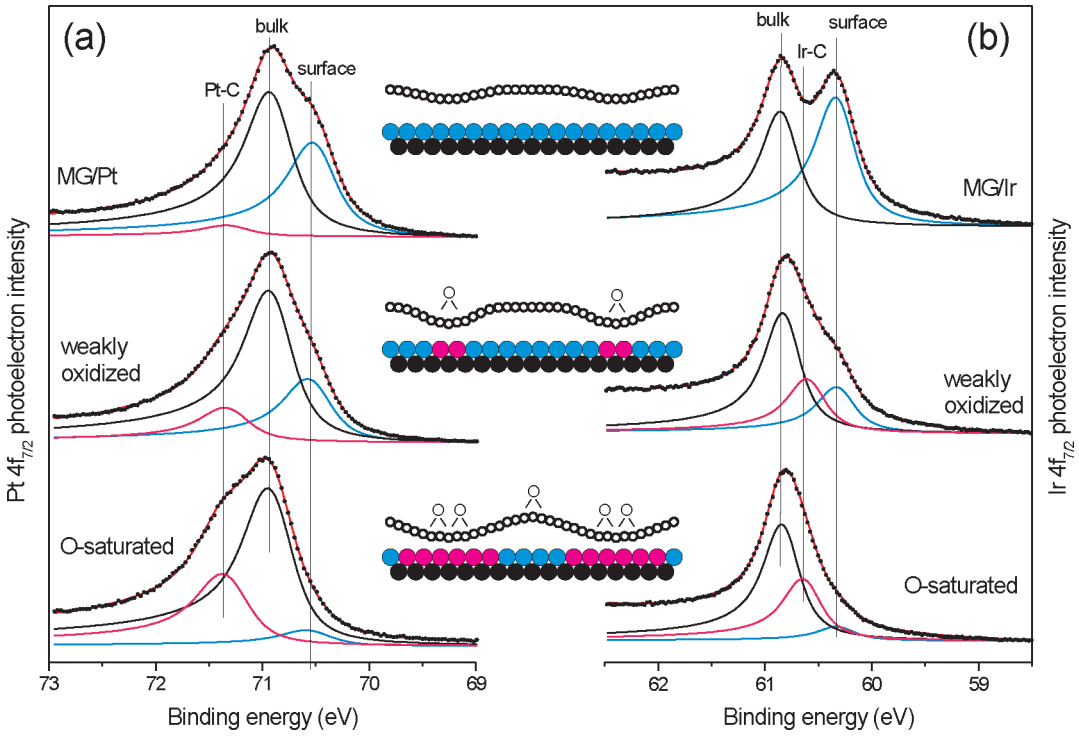

Figure 9. Pt 4f (a) and Ir 4f (b) PE spectra from graphene/TM (TM = Pt or Ir) before and after oxidation with atomic O. "Weakly oxidized" and "O-saturated" situations correspond to the oxidation at the background pressure of 1×10^{-7} mbar for 4 and 30 min, respectively. The inset schematics illustrate growing bonding of C atoms to the substrate as a function of O coverage. Colors of the substrate atoms in the schematics match the colors of the corresponding peak fit components.

With increasing oxygen dose, the moiré structure becomes more distorted and the number of bright protrusions in the pores associated with epoxy groups is also increased (Figure 6c). Although the 6-fold symmetry of the autocorrelation pattern as well as the distance between the spots is conserved (inset), the overall pattern is less sharp than in image (b). On the surface of the oxygen-saturated MG/Ir sample (d), the moiré superstructure becomes completely destroyed at first glance. A lot of bright spots are due to the areas where oxygen is attached to buckled graphene (totally randomized pores). However, the autocorrelation pattern of this image (d, inset) indicates that the original repeating moiré pattern is still preserved, although buried under disorder. The gradual distortion of the nanometer-scale periodicity in MG/Ir upon progressive oxygen adsorption is not surprising. Because of the formation of more sp^3-like bonds at the expense of sp^2-type bonds, the original value of the lattice mismatch between graphene and Ir(111) should not be applicable anymore, due to the increased length of the single C−C bonds. The resulting structure is expected to be buckled in a way similar to sp^3-bonded graphane,[4,55] with hydrogen replaced by oxygen in epoxy groups.

We now turn our attention to the O 1s spectra, shown in Figure 7 for the oxygen-saturated samples of O/HOPG (a), O/MG/Ir(111) (b), and O/MG/Pt(111) (c). The spectra were acquired with a photon energy of 650 eV. For oxygen on HOPG, the spectrum represents a single line with a BE of 531.1 eV, which is consistent with oxygen in epoxy groups, because the BE is lower than that in other O-containing fragments.[54] The same feature at a BE of 531.1 eV is also observed for O/MG/Ir and O/MG/Pt, indicating a similar prevalent mechanism of oxygen−graphene interaction in all samples. However, an extra shoulder can be observed at BEs of 529.0 eV for O/MG/Ir(111) and 529.4 eV for O/MG/Pt(111), denoted as O−Ir and O−Pt, respectively. These peaks can hardly be due to oxygen attached to the point defects and/or grain boundaries in the MG layer, as their BE is lower than the energies typical for carbonyl or ether groups.[54] However, to further evaluate the possibility of O adsorption on point defects, such defects were created in an extra experiment on purpose, by a gentle bombardment of MG/Ir with Ar^+ ions (300 eV, 30 s), following a procedure used for both graphene and HOPG.[44,61] Upon oxygenating the defective film, epoxy groups still dominate the O 1s spectrum (Figure 8, part b), but a new peak arises at the BE of 532.7 eV, which can be reliably attributed to the carbonyl and ether groups formed on point defects in graphene.[44,54] On the other hand, the O−Ir peak gets *weakened* by the introduction of defects. Therefore, it cannot stem from any O-containing species bound to defects. A low BE of this peak, the absence of this peak on graphite, and the 0.4 eV difference in binding energy between MG/Ir and MG/Pt all indicate that the metal substrate has to be involved. We, therefore, tentatively attribute this peak to oxygen atoms penetrating under the graphene, starting from grain boundaries of individual flakes and intercalating between the metal substrates and graphene. This is not a straight oxidation of the metal substrate, as the O adsorption on clean Ir(111) (without graphene) would result in the O 1s BE of 530.0 eV (own data and ref 60), and not 529.0 eV. However, it is plausible to assume that oxygen atoms bound to the metal substrate, but sandwiched between the metal and graphene, can reduce their 1s BE due to the contraction of the O 2p electron density toward the core. Without a direct contact to the metal (like on HOPG), the shoulder at lower BE of the O 1s PE spectrum does not develop (Figure 7, part a).

It is interesting to note that intercalation of atomic oxygen under graphene on Ir is stopped rather early in the oxidation process, as can be seen in Figure 7d, which shows the dynamics of both components in the O 1s PE spectrum upon oxygen treatment of the MG/Ir(111) sample. A similar trend has been observed also for the MG/Pt system (not shown). The component attributed to the intercalated oxygen reaches its saturation limit already at a very early stage of oxidation, at an exposure of about 5 L, while the epoxy-related feature continues to grow with exposures beyond 100 L (more than 17 min) when it also meets the saturation limit. The rapid saturation of the intercalation process may be, in part, due to the substrate temperature being too low (i.e., RT), because, at elevated temperatures, an evidence of oxygen intercalation under graphene on Ir(111) was reported in a recent low-energy electron microscopy study using molecular oxygen.[42] This also hints at another stopping mechanism: in contrast to molecular oxygen, atomic oxygen can also directly bind to the basal plane of graphene, thereby pinning it to the substrate, as discussed above. A gradual increase in the O dose results in a growing number of pinned sites, which suppress excessive intercalation. Similarly, a high defect density (e.g., on the presputtered graphene samples) results in a large amount of O atoms decorating and/or pinning the defects, thus reducing the mobility of oxygen, which is necessary for its intercalation.

Figure 9 shows the evolution of the TM $4f_{7/2}$ core-level component for Pt(111) and Ir(111) upon oxidation. The spectra were taken with a photon energy of $h\nu$ = 120 eV (Ir) and 150 eV (Pt) for maximal surface sensitivity. Initially, the spectra are split into surface- and bulk-related components with BEs of 70.55 and 70.95 eV for Pt(111) and 60.30 and 60.85 eV for Ir(111), respectively. As mentioned in ref 55, the growth of graphene on Pt(111) and Ir(111) does not lead to the reduction or disappearance of the surface-related component in the 4f core-level spectra due to weak interaction of graphene with the 5d metallic substrates and a large distance between them. However, even a moderate oxidation results in a reduction of the surface-related intensity along with the formation of a new detail at higher BE (71.4 eV for Pt and 60.65 eV for Ir). This new interface component is denoted as Pt−C or Ir−C in Figure 9 and is attributed to the regions of the topmost metal layer that are interacting more strongly with carbon atoms due to the pinning of graphene pores by oxygen adsorption. Note also that a direct Ir−O interaction would result in two new components, shifted by −0.20 and +0.23 eV from the bulk peak.[60] The former detail has the same BE as the Ir−C component in Figure 9b, implying that the formation of direct Ir−O bonds cannot be excluded (in agreement with the partial O intercalation proposed above). However, the main contribution to the interface component must be the Ir−C interaction, because we did not observe the second peak characteristic for the Ir−O adsorption.[60] At saturation, the interface component dominates the signal from the topmost substrate layer for both substrates, while the original surface-related component vanishes almost entirely. This is an indication that the buckled area of graphene film extends eventually over almost the entire surface, thus significantly blurring the distinctions between original pores and wires. Besides, partial oxygen intercalation and the formation of Ir−O bonds may contribute to the vanishing of the original surface-related component. The gradual process of pinning graphene to the substrate by oxygen adsorption is illustrated schematically in Figure 9; the color of individual topmost substrate atoms matches the color of the corresponding spectral features. A similar behavior of the substrate core-level spectra was observed upon hydrogenation of graphene on the same metallic substrates,[55] suggesting a universal mechanism of graphene pinning to the 5d metal substrates by active adsorbates.

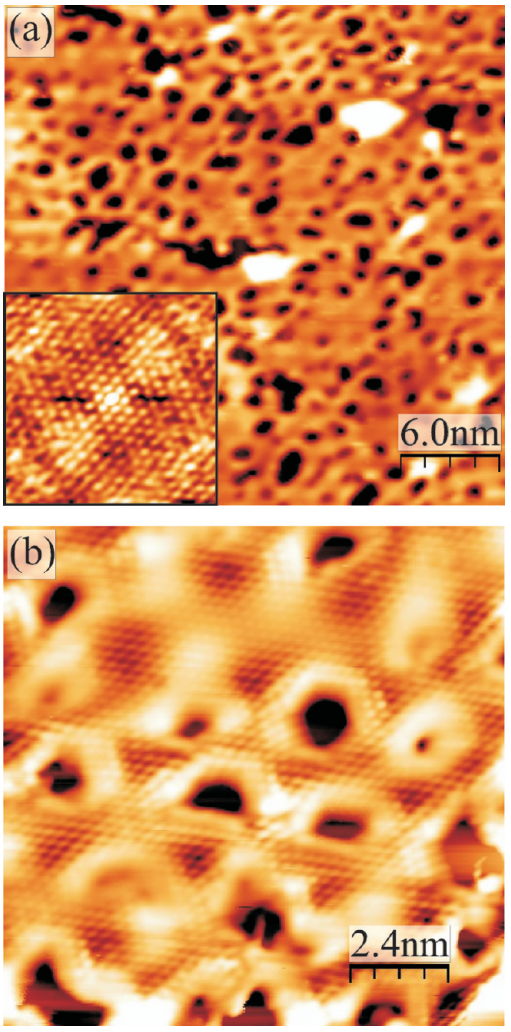

Figure 10. STM images of the MG/Ir(111) sample saturated with atomic O at RT (like in Figure 6d) and annealed to 550 °C (a) and its atomically resolved close-up image (b) showing formation of etched holes in more detail. The autocorrelation pattern of (a) is given as an inset in the bottom-left corner. The tunneling parameters were V_{bias} = 1.6 V, I_t = 200 pA, 30 × 30 nm for (a) and V_{bias} = 30 mV, I_t = 3.3 nA, 12 × 12 nm for (b).

The impact of annealing on the oxygen-saturated MG/Ir(111) sample is demonstrated in the STM images (a) and (b) of Figure 10. The sample annealed at 500 °C shows a highly defective, but nevertheless restored and periodic, moiré pattern, as also evidenced by the autocorrelation image (inset). Image (b) shows a 12 × 12 nm close-up on the distorted moiré pattern. It is clear that the bright protrusions in the pores associated with adsorbed O have disappeared after annealing, indicating a complete desorption of oxygen from the sample, in accordance with our spectroscopic studies. Another fact to support this conclusion is the absence of bright protrusions in the pores associated with the epoxy groups (Figure 6b,c). Numerous defects are observed in the graphene film after annealing, which certainly contribute to the broadening of the C 1s photoemission

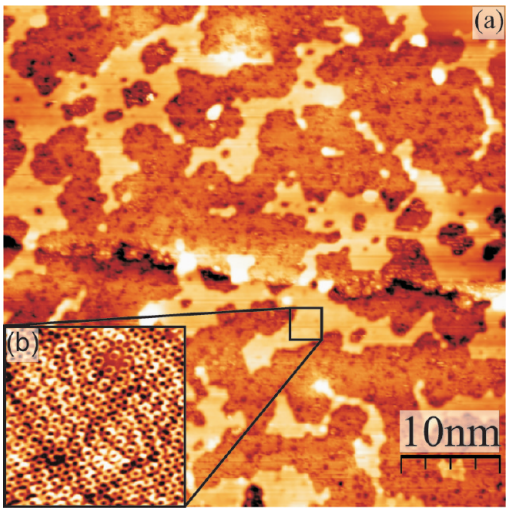

Figure 11. STM image of monolayer graphite grown on the Ir(111) surface treated with atomic oxygen at 300 °C and annealed in UHV at 550 °C (V_{bias} = 1.2 V, I_t = 250 pA, 50 × 50 nm) showing the numerous flat islands of irregular shape on the crystal surface that are the remnants of the graphene film (a). The inset (b) shows the atomically resolved image of one of the islands in (a) within the highlighted area, revealing the graphitic structure (V_{bias} = 15 mV, I_t = 2.8 nA, 5 × 5 nm).

peak in Figure 4 (bottom) and the C 1s NEXAFS π^* and σ^* resonances in Figure 5, spectrum e. These defects are holes punched in graphene due to the oxygen etching at elevated temperatures. Although the autocorrelation pattern is affected by these holes, the sharpness of the spots is comparable to that from the sample with a low oxygen coverage (see Figure 6b). Interestingly, the holes are formed predominantly on the nonbonding wires of the graphene moiré structure, implying that bonding to the substrate makes graphene more resistant to the etching. This results in the fact that many tiny holes can be etched simultaneously, with high concentration and even certain quasi-periodicity. No extended etching fronts could be observed, implying that the mechanism may be different from the intercalation-driven etching typical for molecular oxygen treatment at elevated temperatures.[42] The difference can be attributed to the presence of epoxy groups on the basal plane of our graphene samples prior to the annealing. The surface with a high concentration of tiny etched holes may have a potential as a stable substrate for the growth of small metal particles without agglomeration, for example, for nanocatalysis. On the whole, the process of oxidation is reversible in the sense that O atoms can be removed by annealing, although the remaining graphene monolayer may suffer from a high concentration of tiny etched holes.

To further elucidate the process of oxygen-induced etching, the MG/Ir(111) sample has been treated by atomic O at a temperature of 300 °C and studied by STM. The exposure of oxygen was 90 L, corresponding to a dose of 24 L in the spectroscopic studies (due to the different source-to-sample distance). This procedure promotes oxygen adsorption, intercalation, and desorption of CO and CO_2 simultaneously. The resulting sample has been annealed in UHV at about 550 °C to remove O. Figure 11a shows a typical STM image of the oxygen-etched sample with a number of irregularly shaped small flat islands. In this case, the etching fronts are clearly developed around the islands, while the island surface does not contain many etched holes. The inset (b) of Figure 11 shows a close-up STM image from the highlighted area on one of the islands, confirming that the graphene islands themselves are rather intact. However, no significant moiré contrast could be detected for these remnants of the graphene film, although it was clearly seen in the sample before etching. It is possible that the large perimeter-to-surface ratio of the islands is responsible for this effect; the C atoms on the edges bind to the substrate and tilt down, pushing the center of the island upward. A similar effect was observed for the growth of an intermediate phase between carbidic clusters and graphene on Ir(111), where small (several nanometers in diameter) islands were found to be "dome-shaped" as their edges are strongly interacting with the substrate.[62] On the other hand, it cannot be excluded that some oxygen remains intercalated after annealing, thus contributing to the reduced moiré contrast.

CONCLUSIONS

In situ adsorption of atomic oxygen on MG/Pt(111) and MG/Ir(111) at RT occurs predominantly through the formation of epoxy groups; that is, the oxygen is covalently bonded to a C−C entity, whereby it disturbs the existing carbon sp^2 bonding. The C atoms neighboring the epoxy group will also be forced to adopt a more sp^3 type of bonding, similar to graphane, which can be fulfilled by an increased bonding to the metal substrate. The accommodation of oxygen atoms starts mainly from the "pores" of the moiré structure, where, consequently, also the atomic-scale buckling due to sp^2-to-sp^3 transformation is strongest. The "wires", on the other hand, show a slower uptake of oxygen and, similar to HOPG, do not have the possibility for substrate-assisted buckling. Upon annealing, these regions are most sensitive to oxygen etching, resulting in the formation of small etched holes in the otherwise reasonably restored graphene lattice. This is different from deliberate etching of the MG layer at elevated temperatures, where the resulting MG is fragmented in islands without a moiré pattern instead. Both the selective oxidization of pores/wires and the hole formation can be exploited for selective functionalization or tuning of the electronic properties. Lastly, in the O 1s spectra for oxidized MG on the metal substrates, a second peak is observed at −2.1 (Pt) and −1.7 eV (Ir) below the epoxy O 1s peak. It is not consistent with either metal oxide or oxygen adsorption on defects/grain boundaries in the graphene layer. Instead, it has been assigned to a limited amount of intercalated oxygen atoms. The dynamics of intercalation require a fairly pristine MG layer, and intercalation is halted by adsorption of oxygen on top of the MG, pinning the pores to the substrate.

AUTHOR INFORMATION

Corresponding Author

*E-mail: karina.schulte@maxlab.lu.se (K.S.), alexeip@maxlab.lu.se (A.B.P.).

ACKNOWLEDGMENT

The authors are grateful for the financial support from the Swedish Research Council, the Foundation for Strategic Research (SSF), the Knut and Alice Wallenberg Foundation, the Anna and Edwin Berger Foundation, and the Crafoord Foundation.

REFERENCES

(1) Novoselov, K.; Geim, A. K.; Morozov, S. V.; Jiang, D.; Zhang, Y.; Dubonos, S. V.; Grigorieva, I. V.; Firsov, A. A. *Science* **2004**, *306*, 666.

(2) Lemme, M. C.; Echtermeyer, T. J.; Baus, M.; Kurz, H. *IEEE Electron Device Lett.* **2007**, *28*, 282 and references therein.

(3) Schedin, F.; Geim, A. K.; Morozov, S. V; Hill, E. W.; Blake, P.; Katsnelson, M. I.; Novoselov, K. S. *Nat. Mater.* **2007**, *6*, 652.

(4) Sofo, J. O.; Chaudhari, A. S.; Barber, G. D. *Phys. Rev. B* **2007**, *75*, 153401.

(5) Deng, W.-Q.; Xu, X.; Goddard, W. A. *Phys. Rev. Lett.* **2004**, *92*, 166103.

(6) Zhou, J.; Wang, Q.; Sun, Q.; Chen, X. S.; Kawazoe, Y.; Jena, P. *Nano Lett.* **2009**, *9*, 3867.

(7) Boukhvalov, D. W.; Katnelson, M. I.; Lichtenstein, A. I. *Phys. Rev. B* **2008**, *77*, 035427.

(8) Boukhvalov, D. W.; Katsnelson, M. I. *Phys. Rev. B* **2008**, *78*, 085413.

(9) Elias, D. C.; Nair, R. R.; Mohiuddin, M. G.; Morozov, S. V.; Blake, P.; Halsall, M. P.; Ferrari, A. C.; Boukhvalov, D. W.; Katsnelson, M. I.; Geim, A. K.; Novoselov, K. S. *Science* **2009**, *323*, 610.

(10) Ferro, Y.; Teillet-Billy, D.; Rougeau, N.; Sidis, V.; Morisset, S.; Allouche, A. *Phys. Rev. B* **2008**, *78*, 0854179.

(11) Muradov, N. *Catal. Commun.* **2001**, *2*, 89.

(12) Zhang, Y.; Tang, T.-T.; Girit, C.; Hao, Z.; Martin, M. C.; Zettl, A.; Crommie, M. F.; Ron Shen, Y.; Wang, F. *Nature* **2009**, *459*, 820.

(13) Ritter, K. A.; Lyding, J. W. *Nat. Mater.* **2009**, *8*, 235 and references therein.

(14) Han, M. Y.; Brant, J. C.; Kim, Ph. *Phys. Rev. Lett.* **2010**, *104*, 056801.

(15) Jiao, L.; Zhang, L.; Wang, X.; Diankov, G.; Dai, H. *Nature* **2009**, *458*, 877.

(16) Sprinkle, M.; Ruan, M.; Hu, Y.; Hankinson, J.; Rubio-Roy, M.; Zhang, B.; Wu, X.; Berger, C.; de Heer, W. A. *Nat. Nanotechnol.* **2010**, *5*, 727.

(17) Zhou, S. Y.; Siegel, D. A.; Fedorov, A. V.; Lanzara, A. *Phys. Rev. Lett.* **2008**, *101*, 086402.

(18) Yavari, F.; Kritzinger, C.; Gaire, C.; Song, L.; Gulapalli, H.; Borca-Tasciuc, T.; Ajayan, P. M.; Koratkar, N. *Small* **2010**, *6*, 2535.

(19) Sutter, P.; Sadowski, J. T.; Sutter, E. A. *J. Am. Chem. Soc.* **2010**, *132*, 8175.

(20) Enderlein, C.; Kim, Y. S.; Bostwick, A.; Rotenberg, E.; Horn, K. *New J. Phys.* **2010**, *12*, 033014.

(21) Balog, R.; Jørgensen, B.; Nilsson, L.; Andersen, M.; Rienks, E.; Bianchi, M.; Fanetti, M.; Lægsgaard, E.; Baraldi, A.; Lizzit, S.; Šljivančanin, Ž.; Besenbacher, F.; Hammer, B.; Pedersen, T. G.; Hofmann, P.; Hornekær, L. *Nat. Mater.* **2010**, *9*, 315.

(22) Preobrajenski, A. B.; Ng, M. L.; Vinogradov, A. S.; Mårtensson, N. *Phys. Rev. B* **2008**, *78*, 073401.

(23) Brugger, T.; Günther, S.; Wang, B.; Dil, J. H.; Bocquet, M.-L.; Osterwalder, J.; Wintterlin, J.; Greber, T. *Phys. Rev. B* **2010**, *79*, 045407.

(24) Wintterlin, J.; Bocquet, M.-L. *Surf. Sci.* **2009**, *603*, 1841.

(25) Marchini, S.; Günther, S.; Wintterlin, J. *Phys. Rev. B* **2007**, *76*, 075429.

(26) Sutter, P. W.; Flege, J.-I.; Sutter, E. A. *Nat. Mater.* **2008**, *7*, 406.

(27) Sicot, M.; Bouvron, S.; Zander, O.; Rüdiger, U.; Dedkov, Yu. S.; Fonin, M. *Appl. Phys. Lett.* **2010**, *96*, 093115.

(28) N'Diaye, A. T.; Bleikamp, S.; Feibelman, P.; Michely, T. *Phys. Rev. Lett.* **2006**, *97*, 215501.

(29) N'Diaye, A. T.; Coraux, J.; Plasa, T. N.; Busse, C.; Michely, T. *New J. Phys.* **2008**, *10*, 043033.

(30) Coraux, J.; N'Diaye, A. T.; Engler, M.; Busse, C.; Wall, D.; Buckanie, N.; Meyer zu Heringdorf, F.-J.; van Gastel, R.; Poelsema, B.; Michely, T. *New J. Phys.* **2009**, *11*, 023006.

(31) Sutter, P.; Sadowski, J. T.; Sutter, E. *Phys. Rev. B* **2009**, *80*, 245411.

(32) Loginova, E.; Nie, S.; Thürmer, K.; Bartelt, N. C.; McCarty, K. F. *Phys. Rev. B* **2009**, *80*, 085430.

(33) N'Diaye, A. T.; Gerber, T.; Busse, C.; Mysliveček, J.; Coraux, J.; Michely, T. *New J. Phys.* **2009**, *11*, 103045.

(34) Schniepp, H. C.; Li, J.-L.; McAllister, M. J.; Sai, H.; Herrera-Alonso, M.; Adamson, D. H.; Prud'homme, R. K.; Car, R.; Saville, D. A.; Aksay, I. A. *J. Phys. Chem. B* **2006**, *110*, 8535.

(35) Kosynkin, D. V.; Higginbotham, A. L.; Sinitskii, A.; Lomeda, J. R.; Dimiev, A.; Price, B. K.; Tour, J. M. *Nature* **2009**, *458*, 872.

(36) Loh, K. P.; Bao, Q.; Eda, G.; Chhowalla, M. *Nat. Chem.* **2010**, *2*, 1015.

(37) Paci, J. T.; Belytschko, T.; Schatz, G. C. *J. Phys. Chem. C* **2010**, *111*, 18099.

(38) Liu, L.; Ryu, S.; Tomasik, M. R.; Stolyarova, E.; Jung, N.; Hybertsen, M. S.; Steigerwald, M. L.; Brus, L. E.; Flynn, G. W. *Nano Lett.* **2008**, *8*, 1965.

(39) Lee, S. M.; Lee, Y. H.; Hwang, Y. G.; Hahn, J. R.; Kang, H. *Phys. Rev. Lett.* **1999**, *82*, 217.

(40) Zhang, H.; Fu, Q.; Cui, Y.; Tan, D.; Bao, X. *J. Phys. Chem. C* **2009**, *113*, 8296.

(41) Liao, Q.; Zhang, H. J.; Wu, K.; Li, H. Y.; Bao, S. N.; He, P. *Appl. Surf. Sci.* **2010**, *257*, 82.

(42) Starodub, E.; Bartlet, N. C.; McCarty, K. F. *J. Phys. Chem. C* **2010**, *114*, 5134.

(43) Lee, G.; Lee, B.; Kim, J.; Cho, K. *J. Phys. Chem. C* **2009**, *113* 14225.

(44) Barinov, A.; Malcioglu, O. B.; Fabris, S.; Sun, T.; Gregoratti, L.; Dalmiglio, M.; Kiskinova, M. *J. Phys. Chem. C* **2009**, *113*, 9009.

(45) Sanyal, B.; Eriksson, O.; Jansson, U.; Grennberg, H. *Phys. Rev. B* **2009**, *79*, 113409.

(46) Li, J.-L.; Kudin, K.; McAllister, M. J.; Prud'homme, R. K.; Aksay, I. A.; Car, R. *Phys. Rev. Lett.* **2006**, *96*, 176101.

(47) Incze, A.; Pasturel, A.; Peyla, P. *Phys. Rev. B* **2004**, *70*, 212103.

(48) Wehling, T. O.; Katsnelson, M. I.; Lichtenstein, A. I. *Phys. Rev. B* **2009**, *80*, 085428.

(49) Nakamura, J.; Ito, J.; Natori, A. *J. Phys.: Conf. Ser.* **2008**, *100* 052019.

(50) Yan, J.-A.; Chou, M. Y. *Phys. Rev. B* **2010**, *82*, 125403.

(51) Xu, Z.; Xue, K. *Nanotechnology* **2010**, *21*, 045704.

(52) Erickson, K.; Erni, R.; Lee, Z.; Alem, N.; Gannett, W.; Zettl, A. *Adv. Mater.* **2010**, *22*, 4467.

(53) Horcas, I.; Fernández, R.; Gómez-Rodríguez, J. M.; Colchero, J.; Gómez-Herrero, J.; Baro, A. M. *Rev. Sci. Instrum.* **2007**, *78*, 013705.

(54) Jordan, J. L.; Kovac, C. A.; Morar, J. F.; Pollack, R. A. *Phys. Rev. B* **1987**, *36*, 1369.

(55) Ng, M. L.; Balog, R.; Hornekær, L.; Preobrajenski, A. B.; Vinogradov, N. A.; Mårtensson, N.; Schulte, K. *J. Phys. Chem. C* **2010**, *114*, 18559.

(56) Paci, J. T.; Upadhyaya, H. P.; Zhang, J.; Schatz, G. C.; Minton, T. K. *J. Phys. Chem. A* **2009**, *113*, 4677.

(57) Prince, K. C.; Richter, R.; de Simone, M.; Alagia, M.; Coreno, M. *J. Phys. Chem. A* **2003**, *107*, 1955.

(58) Pandey, D.; Reifenberger, R.; Piner, R. *Surf. Sci.* **2008**, *602*, 1607.

(59) Solís-Fernández, P.; Paredes, J. I.; López, M. J.; Cabria, I.; Alonso, J. A.; Martínez-Alonso, A.; Tascón, J. M. D. *J. Phys. Chem. C* **2009**, *113*, 18719.

(60) Bianchi, M.; Cassese, D.; Cavallin, A.; Comin, R.; Orlando, F.; Postregna, L.; Golfetto, E.; Lizzit, S.; Baraldi, A. *New J. Phys.* **2009**, *11*, 063002.

(61) Lehtinen, O.; Kotakoski, J.; Krasheninnikov, A. V.; Tolvanen, A.; Nordlund, K.; Keinonen, J. *Phys. Rev. B* **2010**, *81*, 153401.

(62) Lacovig, P.; Pozzo, M.; Alfe, D.; Vilmercati, P.; Baraldi, A.; Lizzit, S. *Phys. Rev. Lett.* **2009**, *103*, 166101.